Results in Engineering 24 (2024) 103411

Contents lists available at ScienceDirect

Results in Engineering

journal homepage: www.sciencedirect.com/journal/results-in-engineering

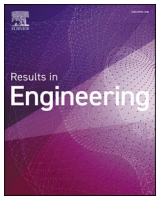

Research paper

A compact microstrip antenna with dual thin slits for high-capacity data streaming in the 38 and 39 GHz bands for 5G applications

AbdulGuddoos S.A. Gaid [a,*], Ala'a N.S. Ali [a], Mohammad Ahmed Alomari [b]

[a] Communication & Computer Engineering Dept., Faculty of Engineering & Information Technology, Taiz University, Taiz, Yemen
[b] Engineering Technology Dept., Faculty of Technology & Electronic and Computer Engineering (FTKEK), Universiti Teknikal Malaysia Melaka (UTeM), Melaka, Malaysia

ARTICLE INFO

Keywords:
Wideband antennas
Slits
High-gain
5G
38GHz and 39GHz bands
CST
HFSS

ABSTRACT

This article presents a simple rectangular microstrip antenna for 5G applications in the 38 and 39 GHz bands. The antenna prioritizes broad bandwidth and high gain for efficient signal transmission. It features a compact design, printed on a Rogers RT/Duroid 5880 substrate with dimensions of 5 × 8.2 × 0.186 mm^3 ($\varepsilon_r = 2.2$ and $\tan\delta = 0.0009$) and includes two thin slits integrated with the radiating patch. This configuration achieved an impressive 3.11 GHz impedance bandwidth, covering a broad spectrum from 37.23 GHz to 40.34 GHz. Additionally, the radiation gain ranges from 6.55 dBi at the band's upper frequency to 9.03 dBi at the lower frequency, with a value of 9.03 dBi at the primary operational frequency of 38 GHz. The radiation efficiency remains nearly consistent across the operational frequencies, ranging from 86.97 % at the upper end to 88.96 % at the lower end, with an efficiency of 88.29 % at 38 GHz. Moreover, the antenna exhibits excellent matching to its feed, as demonstrated by the minimal value of 1.012 for Voltage Standing Waves Ratio (VSWR) and the low S_{11} parameter value of -60 dB at the 38 GHz frequency. The proposed antenna was designed and optimized using the Computer Simulation Technology (CST) simulator, while its performance was verified with the High-Frequency Structure Simulator (HFSS). The results from both simulators align remarkably well. This antenna design demonstrated promising bandwidth and radiation characteristics, making it well-suited for 5G applications.

1. Introduction

The launch of 5G mobile networks marks a critical turning point in high-speed wireless communication systems. These networks, with the potential to revolutionize data transmission and connectivity, can accommodate the ever-increasing demands for data required by the mobile market. Compared to 4 G, these networks promise a jump to much faster data speeds, ensuring ubiquitous connectivity. Nevertheless, there are significant challenges in network specifications and antenna systems that need to be addressed to match the expanding capacity and data rate needs [1–4].

5G communication systems employ the millimeter wave spectrum, which offers several benefits, such as wide bandwidth, qualifying for high-speed transfer, and low latency. In addition, less congestion in this frequency range enhances network performance. Nonetheless, using this frequency spectrum poses some challenges, including high signal attenuation due to path loss, the atmospheric absorption of signals, and signal losses caused by rain. Moreover, the signal coverage area is limited in this frequency region. Consequently, allocating millimeter wave frequencies for 5G communication networks requires careful planning to ensure reliable operation. It is also crucial to optimize communication networks and effectively design antenna systems that minimize signal losses and provide adequate coverage [5–9].

To address the challenges associated with millimeter-wave frequencies, scholars explored the potential of microstrip antenna technology. This technology has shown considerable promise for integration into 5G systems, both in fixed stations or mobile units, especially for tasks like beamforming or establishing MIMO arrays [10]. This technology is well-suited for various applications due to its compactness, lightweight, low cost, and simplicity of manufacturing [11–13]. However, they are limited by factors such as narrow bandwidth, low efficiency, and modest gain. In response, researchers have proposed various approaches, including the use of metamaterials, slot etching, integration of slits, implementation of partial ground structures, and utilization of

* Corresponding author.
E-mail addresses: quddoos.gaid@taiz.edu.ye (A.S.A. Gaid), alomari@utem.edu.my (M.A. Alomari).

https://doi.org/10.1016/j.rineng.2024.103411
Received 28 July 2024; Received in revised form 9 November 2024; Accepted 12 November 2024
Available online 14 November 2024

defective ground structures (DGS). These methods intend to design microstrip antennas with broad bandwidth and directional control for transmitting and receiving signals [14,15].

Researchers have extensively investigated microstrip antennas for 5G, particularly around the 38 and 39 GHz bands [16–28]. These studies explore both single and multi-band designs to optimize performance. For instance, a design that operates in the 28/38 GHz bands was discussed in [16]. This design achieved a gain of 6.6 dBi and a 1.23 GHz bandwidth at 38 GHz. Another study proposed a monopole antenna with triangular stubs for 28 GHz and 38 GHz operation [17]. This antenna exhibited two bands (25.9 - 30.4 GHz and 36.4 - 40.2 GHz) with peak gains of 4.54 dBi and 4.21 dBi, demonstrating its potential for 5G data transmission. Another investigation [18] examined a compact, 15 × 25 × 0.25 mm^3, dual-band microstrip antenna for 38/60 GHz. This design, utilizing a microstrip line for power and implemented on a Rogers RO3003TM substrate (ε_r = 3, tan δ = 0.001), achieves significant bandwidths of 3.2 GHz at 60 GHz and 2.0 GHz at 38 GHz. It also reported good reflection coefficient values (−42 dB, −47 dB) and decent peak gains (6.5 dBi, 5.5 dBi) in the two bands.

Moreover, the work in [19] investigated a design featuring an altered circular patch alongside a parasitic element. This configuration enabled operation in both the 28 GHz and 38 GHz bands. The structure, built on Rogers RO3003™ substrate ($\varepsilon_r = 3$) remained compact with a size of 7.5 × 8.8 × 0.25 mm^3. Within the 38 GHz band, it achieved a reflection coefficient of −27.3 dB, a 1.06 GHz bandwidth, and a maximum gain of 5.86 dBi. The design outlined in [20] illustrated a compact antenna specifically for the 38 GHz band. This design (12 × 12 × 0.203 mm^3) combined a circular patch integrated with a rectangular slot and grounded by a partial plane. It achieved a good balance of properties with a notable 3 GHz bandwidth, a reflection coefficient of −30 dB, and a gain of 5.5 dBi.

Furthermore, the authors of [21] proposed an HP-shaped design to cover the (36.83 - 40 GHz) range. This design, made on a 23.7 × 8.8 × 0.51 mm^3 Rogers RT5880 substrate, impressed with a low reflection coefficient of around −33 dB, a good gain of 6.5 dBi, a broad bandwidth of 3.17 GHz, and efficient radiation of 80 %. Another work [22] investigated a single-band, two-pronged fork-shaped antenna for 38.5 GHz. This design with a 10 × 6 × 0.254 mm^3 Rogers RT5880 substrate, achieved a good S_{11} of −30 dB, but with a trade-off of a narrower bandwidth (<2 GHz) for a higher peak gain (7.6 dBi).

In addition, the study in [23] outlined a compact U-shaped antenna fed by a transmission line (10 × 6 × 0.254 mm on Rogers RT5880 substrate). It achieved a good balance between bandwidth (around 1 GHz centered at 37 GHz) and gain (6.84 dBi) with a good reflection coefficient (−20 dB). The work presented in [24] explored a rectangular patch antenna with slits for a wide bandwidth extending from 36.65 GHz to 40.22 GHz. It achieved good reflection coefficients at the two resonance frequencies (around −32 dB and −18 dB).

The research in [25] suggested a small structure with a rectangular shape to work at 38 GHz. This design employed Rogers RT Duroid 5880 substrate and achieved a good balance between bandwidth and gain. The design produced a bandwidth of 2.35 GHz centered at 38.67 GHz, a high gain of 8.04 dBi, and an efficient radiation of almost 99 % across the operational band. Finally, the study in [26] discussed a tri-band antenna for the key 5G frequencies (28 GHz, 38 GHz, and 60 GHz) on a compact substrate (8 × 8.5 × 0.508 mm^3). This antenna achieved good performance across all bands with low reflection coefficients, good bandwidths, over 1 GHz in each band, and high peak gains, of >6 dBi. It also maintained high radiation efficiencies throughout the operating range.

The antenna designs referenced in [29–38] operate within the 36 GHz to 42 GHz frequency range, with several supporting dual-mode functionality, often incorporating the 28 GHz and 26 GHz bands. These designs include both MIMO and single antenna configurations and employ techniques such as slots, slits, and DGS (Defected Ground Structures) to enhance performance. Although their wide bandwidth is a significant strength, vital for high-data-rate communications, these antennas face some limitations. Many exhibit only moderate gain and relatively large physical sizes, which makes them less suitable for compact or space-constrained applications.

For 5G smart devices, where space and power are limited, antennas need to be both compact and efficient. At millimeter-wave frequencies like 38 GHz, significant path loss occurs, making high gain crucial for strong signal transmission and reception. The proposed antenna must be compact enough to fit within the limited space of smart devices while delivering adequate gain to compensate for path loss. It also needs to support wide bandwidths to handle the high data rates required by 5G networks. One major drawback of many designs discussed above is their low gain, which weakens signal strength and reduces overall performance. Additionally, their larger sizes make them unsuitable for compact devices that are becoming more common in modern wireless systems. Furthermore, many designs show moderate return loss, indicating suboptimal impedance matching and leading to power reflection, reducing system efficiency. Poor VSWR also affects performance in high-frequency applications. To meet the compactness, efficiency, and performance requirements of 5G networks, antenna designs must overcome these limitations in gain, size, and impedance matching.

This study introduces a compact microstrip patch antenna measuring 5 × 8.2 × 0.186 mm^3, constructed on a Rogers RT Duroid substrate with a relative permittivity of 2.2 and a loss tangent of 0.0009. Designed for 5G applications within the 38 and 39 GHz bands, the antenna incorporates two thin rectangular slits to enhance its performance. It achieves a peak gain of 9.03 dBi, a wide bandwidth of 3.11 GHz, and impressive reflection coefficients of −60 dB at 38 GHz and −32 dB at 39.8 dB, ensuring efficient power transfer and signal transmission. The design and performance were validated using CST and HFSS, industry-standard electromagnetic simulation tools based on the Finite Integration Technique (FIT) and Finite Element Method (FEM), respectively.

The remainder of this manuscript is structured as follows: Section II offers a meticulous examination of the design methodology of the proposed antenna. Section III investigates how variations in specific antenna parameters influence the reflection coefficient performance. Building upon the initial simulations, Section IV presents supplementary data on various antenna characteristics alongside the critical verification process using the HFSS simulator. Finally, Section V summarizes the paper's key achievements and outlines potential avenues for further research endeavors.

2. The proposed design geometry

This part explores the design and optimization stages of a microstrip patch antenna proposed for 5G applications in the 37.23 - 40.34 GHz range, comprising the 38 and 39 GHz bands. The design employs a rectangular patch on a Rogers RT/Duroid 5880 substrate ($\varepsilon_r = 2.2$, tan δ = 0.0009, hs = 0.186 mm) with a full ground plane (0.043 mm thick copper sheet) for efficient radiation within the specified band.

A meticulous three-phase design approach was implemented, leveraging electromagnetic simulations using CST software to refine the antenna's performance. Initial rectangular patch dimensions were established using existing formulas in the literature [2], considering the target operating frequency (38 GHz), substrate properties, and the desired size. Subsequent simulations in CST software were conducted to fine-tune these dimensions, achieving a preliminary resonant frequency of 37.6 GHz, close to the target center frequency.

Following the initial design, the focus shifted towards optimizing the antenna's reflection coefficient for a broader bandwidth and efficient signal transmission across the band. To achieve these enhancements, two identical thin rectangular slits were strategically integrated into the leading edge of the radiating patch. Iterative simulations using CST software determined the optimal slit configuration, balancing improvements in impedance bandwidth, resonant frequency precision, and reflection coefficient. Fig. 1 illustrates the final design with its optimized

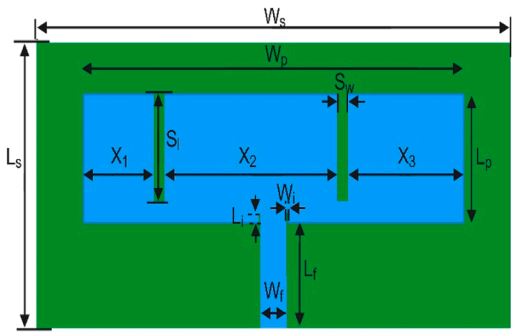

Fig. 1. Geometry of the optimized proposed design.

dimensions ($L_s \times W_s \times hs = 5 \times 8.2 \times 0.186$ mm^3). The figure depicts a microstrip transmission line ($L_f = 1.8$ mm, $W_f = 0.5$ mm) feeding the radiating element ($L_p \times W_p = 2.42 \times 6.8$ mm^2). An inset feed with length, $L_i = 0.218$ mm, and width, $W_i = 0.1$ mm, ensures optimal coupling between the feed line and the patch.

Fig. 2 depicts the simulated reflection coefficients (S_{11} parameter) for the proposed antenna across the three main design phases. The S_{11} parameter is crucial for evaluating impedance matching between the feed line and the radiating patch, directly impacting the antenna's power transfer efficiency and its operational bandwidth. Additionally, each design phase reflects the current distribution across the patch surface, which in turn influences the antenna's radiation characteristics. The specific details of the design and optimization process are outlined below:

- Phase 1: The initial design featured a simple rectangular patch configuration without any additional modifications. This configuration resonated at 37.6 GHz, but the reflection coefficient was somewhat moderate, measuring −15.97 dB with a bandwidth of approximately 1.34 GHz, as shown in Fig. 2. Fig. 3(a) illustrates the evenly distributed current density across the radiating element, with the current flowing uniformly in the same direction. This contributed to enhanced radiation performance, resulting in a high gain of around 9.12 dBi, as depicted in Fig. 3(b and c). However, despite these favorable characteristics, further optimization was needed to improve impedance matching, increase the bandwidth, and precisely tune the resonance to 38 GHz to achieve optimal performance for the intended application.
- Phase 2: In an attempt to enhance the reflection coefficient and overall performance, a single rectangular slit was introduced along the longitudinal axis of the radiating patch. The slit was optimized

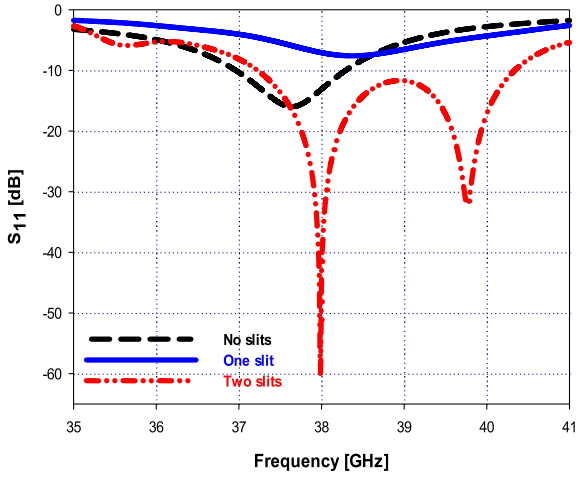

Fig. 2. Simulated S_{11} performances for different design phases.

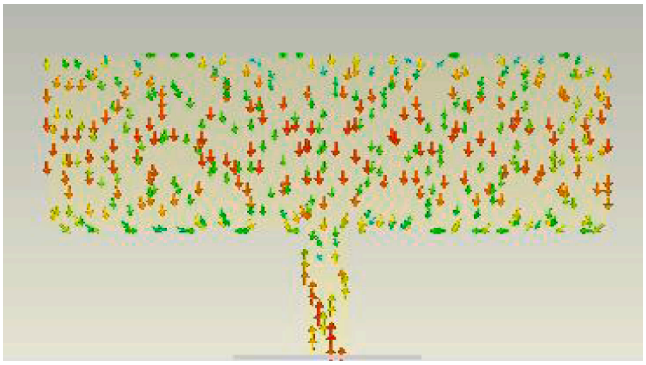

(a)

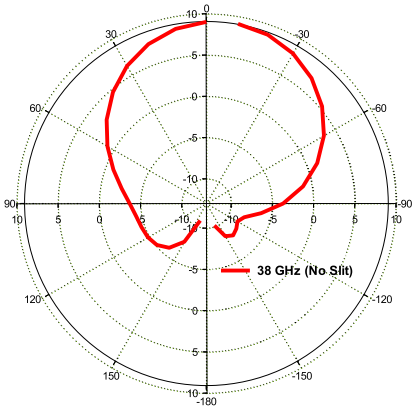

(b)

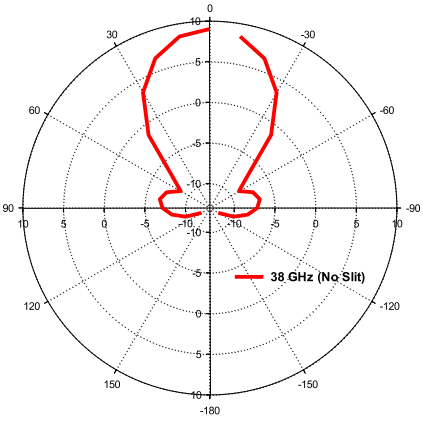

(c)

Fig. 3. Surface current density and 2D radiation patterns at 38 GHz with no slits (a) Current distribution, (b) E-Plane, and (c) H-Plane.

with dimensions of Sw = 0.2 mm and Sl = 2.02 mm, positioned 1.3 mm from the left edge (X1). Unfortunately, this modification resulted in a further decline in the reflection coefficient, with no bandwidth achieved for S11 ≤ −10 dB. Additionally, the current distribution became imbalanced. As shown in Fig. 4(a), the current was more concentrated on the right side of the patch, while the left side experienced reduced current density. The current flow directions were also inconsistent, causing destructive interference between the radiated fields, which reduced the gain to 6.94 dBi (at θ = 0o), as illustrated in Fig. 4(b and c). Consequently, further adjustments were required to address these performance issues.

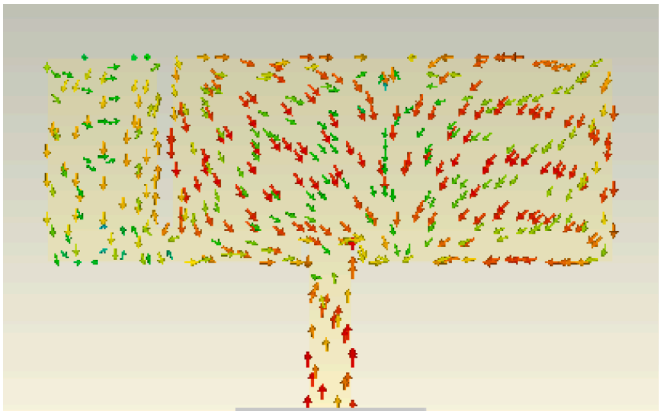

(a)

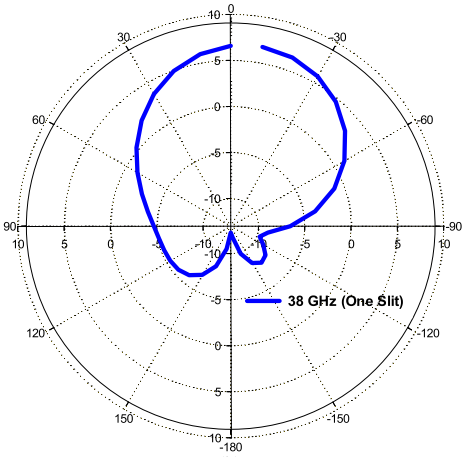

(b)

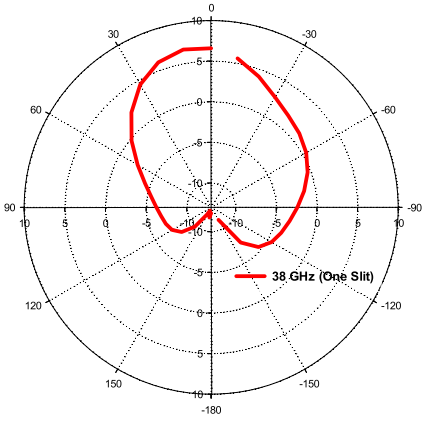

(c)

Fig. 4. Surface current density and 2D radiation patterns at 38 GHz with the left slit (a) Current distribution, (b) E-Plane, and (c) H-Plane.

- Phase 3: To resolve the issues encountered in Phase 2, a second identical rectangular slit was introduced, positioned 2.2 mm from the right edge (X3) of the patch. This addition was intended to optimize the current distribution across the radiating element, enhancing impedance matching, expanding bandwidth, and improving radiation characteristics. The introduction of the two slits led to a significant improvement in the antenna's performance. The design now exhibited two resonant frequencies: a primary resonance at 38 GHz and a secondary resonance at 39.8 GHz. The reflection coefficient improved markedly at both frequencies, with values of −60 dB at 38 GHz and −32 dB at 39.8 GHz, and the bandwidth increased to 3.11 GHz, as shown in Fig. 2.

At the primary resonance of 38 GHz, Fig. 5(a) shows that the current density is highest on the left and middle portions of the patch, with the currents now aligned and moving in the same direction, resulting in minimal destructive interference between the radiated fields. This improvement in current distribution enhanced the radiation performance, resulting in a gain of 9.027 dBi (at $\theta = 0°$), as depicted in Fig. 5(b and c). Though the gain decreased slightly from 9.12 dBi to 9.027 dBi, the substantial improvements in reflection coefficient and bandwidth

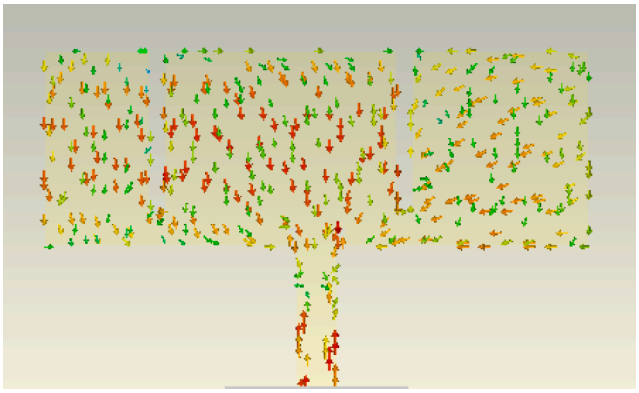

(a)

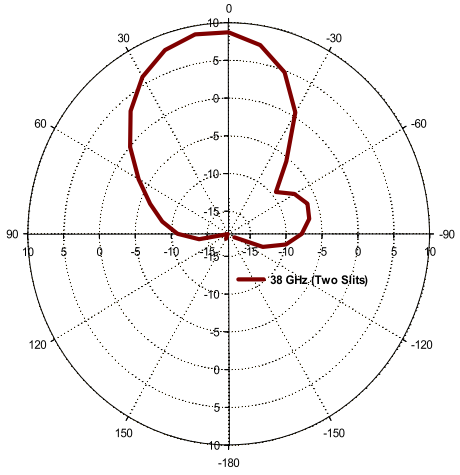

(b)

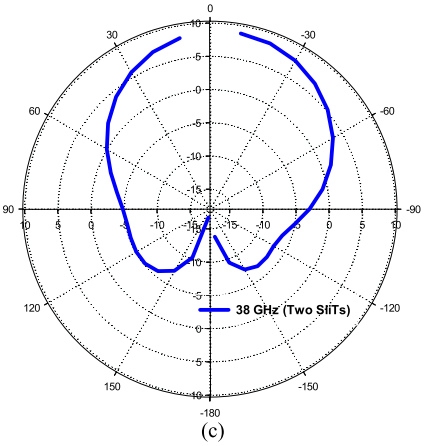

(c)

Fig. 5. Surface current density and 2D radiation patterns at 38 GHz with two slits (a) Current distribution, (b) E-Plane, and (c) H-Plane.

more than compensated for this minor loss, significantly boosting the antenna's efficiency and signal transmission quality.

At the secondary resonance of 39.8 GHz, Fig. 6 portrays the current distribution and radiation characteristics. As shown in Fig. 6(a), the current is more concentrated on the right and middle portions of the patch, with most currents flowing in opposite directions, except for those near the right edge of the patch and the right edge of right slit, which aligned. The opposing currents adversely impacted the radiation patterns, causing a reduction in gain to around 7.3 dBi, with the main lobe skewed to the left of the boresight, as shown in Fig. 6(b and c).

In summary, through these three design phases, the proposed antenna underwent critical transformations that improved its impedance matching, expanded its operational bandwidth, and optimized its radiation characteristics. The final design strikes a balance between high gain and excellent reflection coefficient, ensuring it meets the rigorous demands of 5G communication systems.

Fig. 7 further strengthens the analysis by illustrating the input impedance (Z_{11}) of the proposed antenna throughout the designated operating band. As observed in the figure, the input impedance closely approaches 50 Ω at both resonant frequencies (38 GHz and 39.8 GHz). This indicates that the antenna is well-matched to its power feeder, ensuring efficient power transfer and minimal signal reflection within the antenna.

3. Study of antenna parameters

In this section, we explore how key antenna parameters like substrate height, slit dimensions (length and width), and slit placement (relative to the patch edges) affect the S_{11} performance of the proposed design. By simulating how variations in these parameters influence performance, this section aims to provide design guidelines for optimizing the antenna.

3.1. Effects of varying height (hs) of the dielectric substrate

Fig. 8 highlights the critical role of varying height (hs) of the dielectric substrate on the S_{11} performance of the suggested antenna. A height of 0.186 mm is ideal, achieving resonance at 38 GHz (the primary resonant frequency) and a good impedance match (−60 dB for S_{11}). Deviations from this value degrade the performance: increasing hs leads to a shift in resonance frequency down and reduces S_{11} while decreasing hs pushes resonance frequency up and reduces S_{11} too. This emphasizes the importance of choosing the right hs for optimal resonance, bandwidth, and S_{11} performance.

3.2. Effects of varying the width (S_w) and length (S_l) of the slits

Fig. 9 examines the impact of slits' width (S_w) on the S_{11} performance of the design, identifying 0.2 mm as the optimal value for maximizing return loss and impedance bandwidth. This width ensures efficient signal reflection and a broader operating range, while deviations from 0.2 mm degrade the reflection coefficient and reduce return loss. Similarly, Fig. 10 investigates the effect of varying slits' length (S_l). Deviating from the optimal S_l of 2.02 mm disrupts the intended resonance behavior, shifting the resonance frequency away from the desired 38 GHz and diminishing performance within the band. This shift often results in decreased return loss, indicating poorer impedance matching, increased signal reflection, and reduced power transfer efficiency.

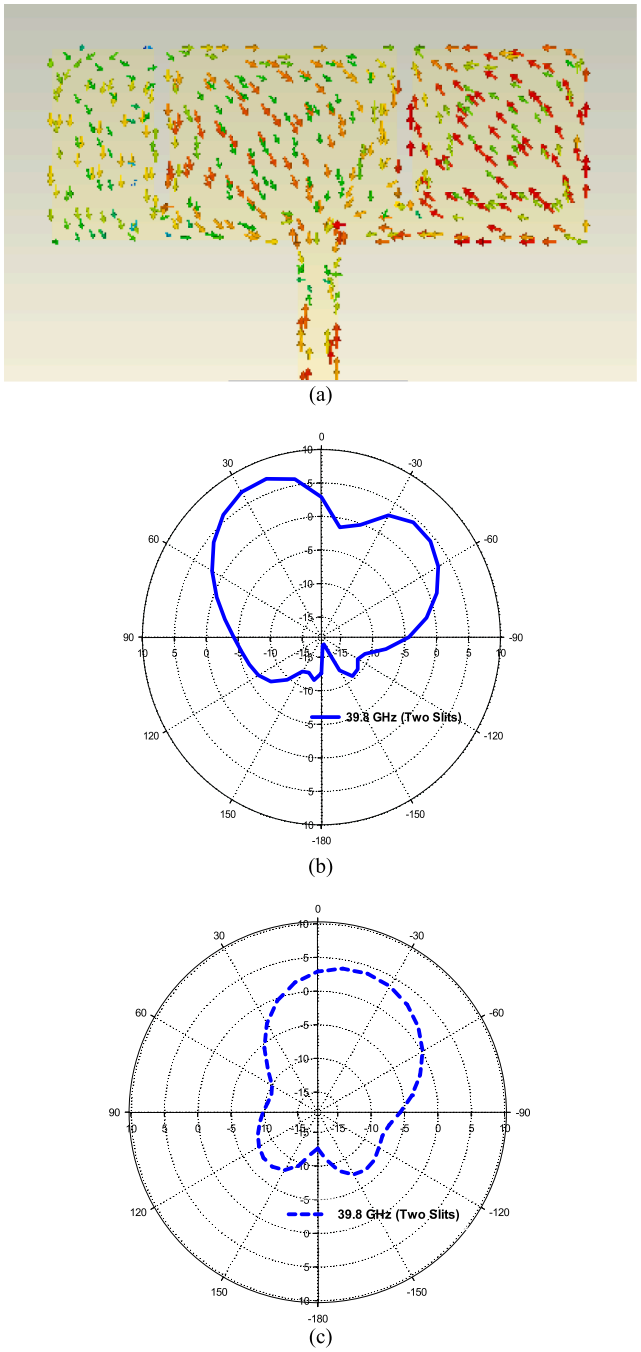

Fig. 6. Surface current density and 2D radiation patterns at 39.8 GHz with two slits (a) Current distribution, (b) E-Plane, and (c) H-Plane.

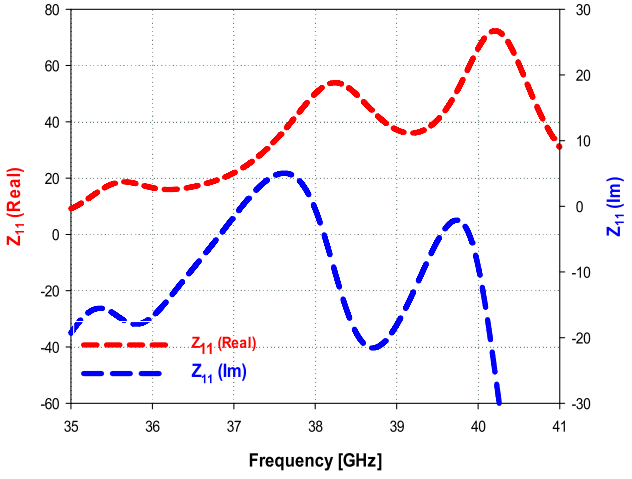

Fig. 7. The input impedance (Z_{11}) of the optimized antenna vs the operating frequencies.

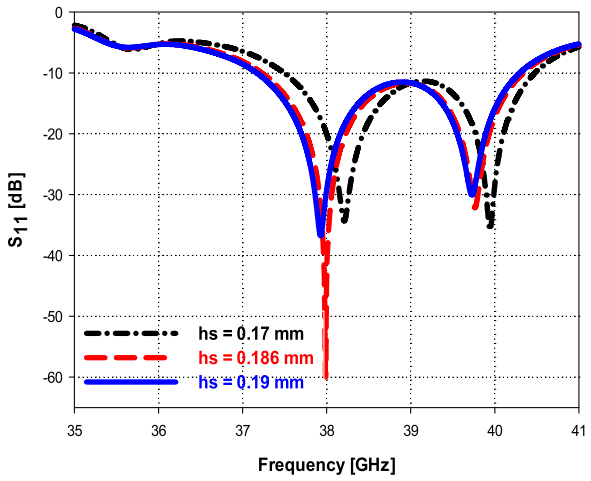

Fig. 8. Effects of varying the substrate height (hs) on the S_{11} performance.

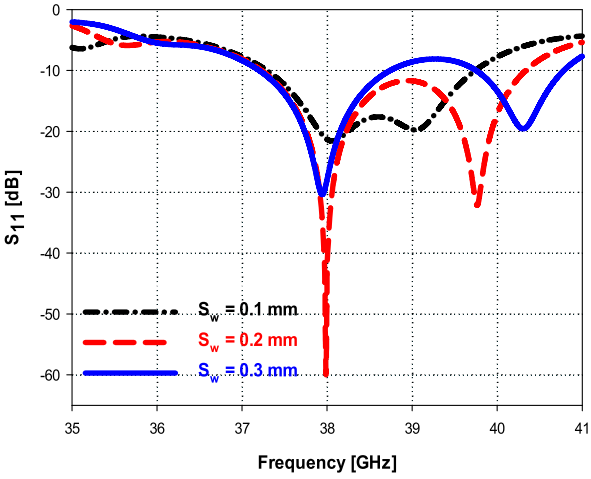

Fig. 9. Effects of varying the slits' width (S_w) on the S_{11} performance.

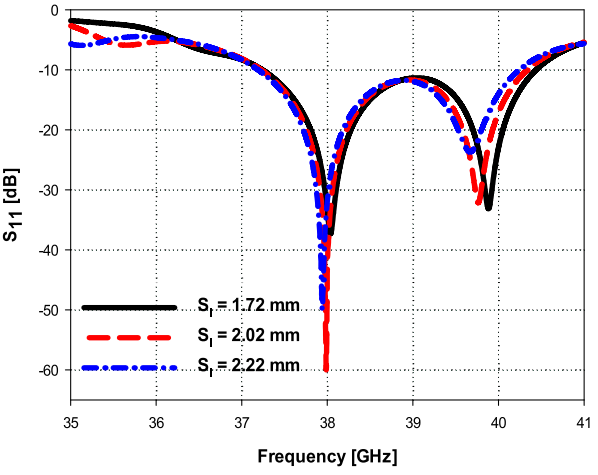

Fig. 10. Effects of varying the slits' length (S_l) on the S_{11} performance.

Furthermore, Fig. 11 plots the reflection coefficient performance when varying S_l and S_w at the same time. The curves show that the optimal performance is obtained for $S_l = 2.02$ mm and $S_w = 0.2$ mm. This result confirms the results shown in Figs. 9 and Fig. 10.

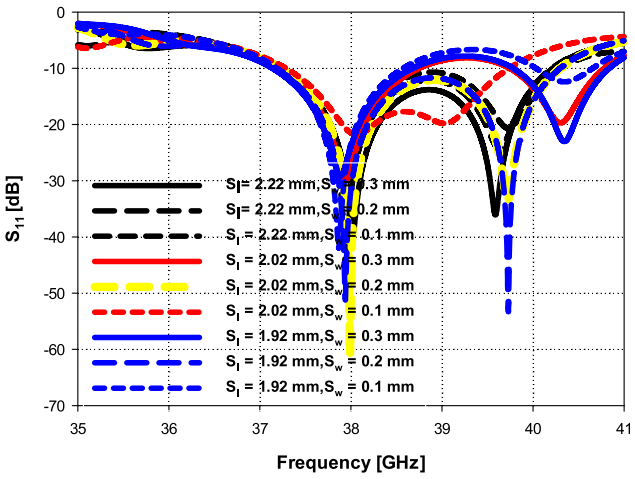

Fig. 11. Joint effect of varying S_w and S_l on the S_{11} performance.

3.3. Joint effects of varying S_l and X_1

Fig. 12 depicts the influence of varying the values of S_l and X_1 simultaneously on the reflection coefficient performances. It is clearly noted that the optimal performance is obtained for $S_l = 2.02$ mm and $X_1 = 1.3$ mm.

3.4. Effects of varying the slit's positions (X_1 and X_3)

Fig. 13 illustrates the influence of left slit position (X_1) relative to the patch edge. An optimal X_1 of 1.3 mm is crucial for achieving the desired dual resonances at 38 GHz and 39.8 GHz with good return loss values of 60 dB and 32 dB, respectively. Moving the slit away from this optimal position will cause the resonance frequency to drift and the signal reflection to worsen. Likewise, Fig. 14 explores the impact of the right slit position (X_3). An optimal X_3 of 2.2 mm is important for ensuring the antenna is well-matched with efficient signal reflection. Deviations from this value may require further design adjustments to maintain optimal performance within the band. Moreover, varying the dimensions of X_1 and X_3 together results in the reflection coefficient curves portrayed in Fig. 15. From this figure, it is clearly noticed that the optimal performance is reached when $X_1 = 1.3$ mm and $X_3 = 2.2$ mm.

4. Simulation results: validation and discussion

The proposed structure was designed and optimized using CST

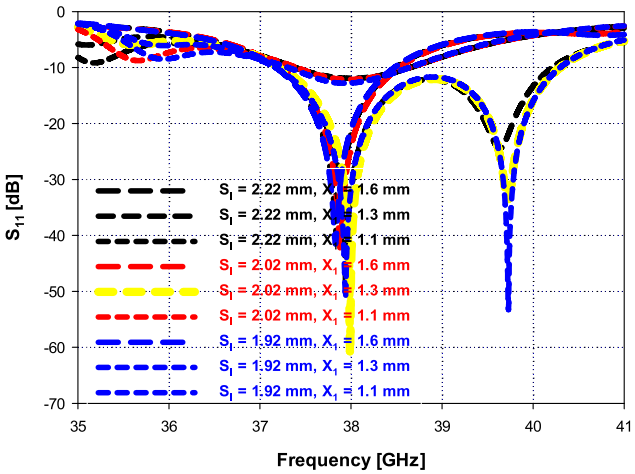

Fig. 12. Joint effects of S_l and X_1 on the S_{11} performance.

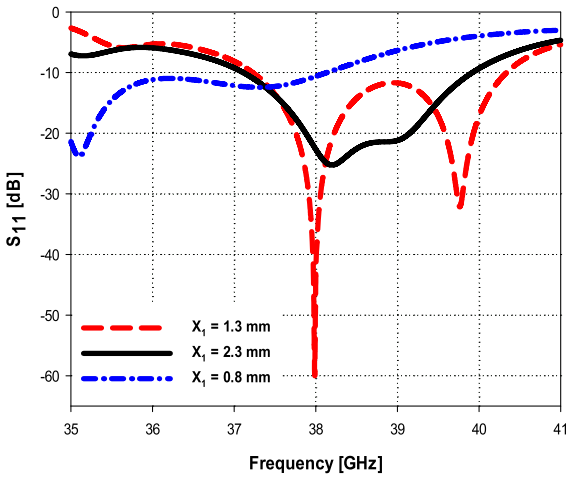

Fig. 13. Effects of varying X_1 on the S_{11} performance.

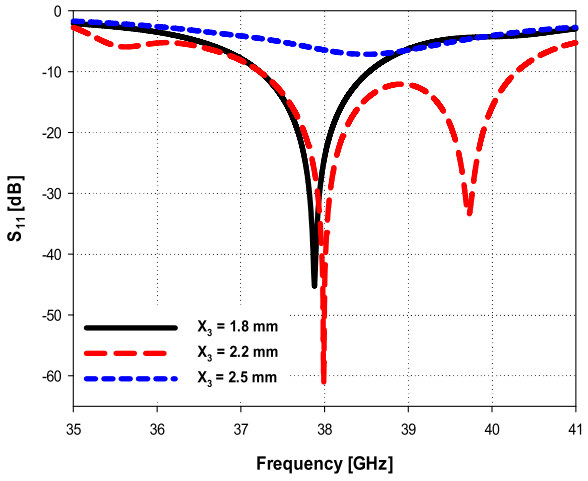

Fig. 14. Effects of varying X_3 on the S_{11} performance.

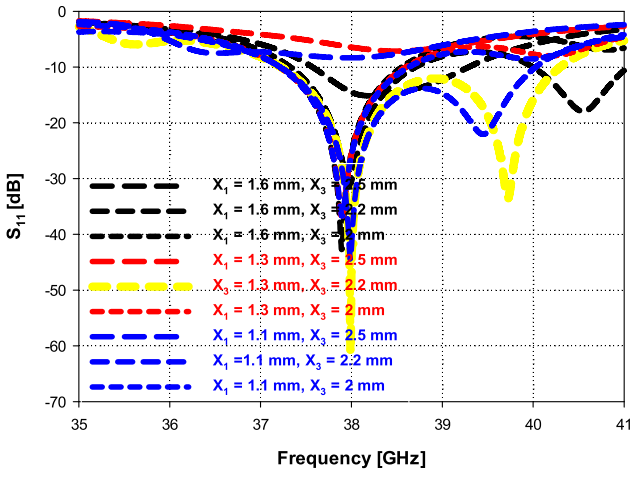

Fig. 15. Joint effects of varying X_1 and X_3 on the S_{11} performance.

software. To verify the results and enhance confidence in the design's performance, the final design was also simulated using HFSS software. The excellent agreement between CST and HFSS simulations validates the antenna design and reduces the risk of unexpected behavior during fabrication. This combined approach with CST and HFSS offers a more comprehensive understanding of the antenna's performance across its operating bands. This section compares the various performance metrics of the proposed antenna obtained from both CST and HFSS simulations.

4.1. The S_{11} performance

Fig. 16 compares the S_{11} performance of the antenna as obtained from CST and HFSS simulations. Both curves show excellent agreement: CST achieves 60 dB return loss at 38 GHz (primary resonance) and 32 dB at 39.8 GHz (secondary), with a 3.11 GHz bandwidth. HFSS shows 59 dB return loss at a slightly shifted resonance to 38.1 GHz and 28 dB at 40.1 GHz, with a wider 3.3 GHz bandwidth (37.4 GHz to 40.7 GHz). These minor discrepancies are within acceptable limits due to differences in simulation software models. The strong overall agreement validates the proposed antenna design.

4.2. The VSWR

Fig. 17 exhibits the VSWR characteristics from both CST and HFSS simulations. They again exhibit excellent agreement. CST results show VSWR of 1.012 at 38 GHz and 1.01 at 39.8 GHz, while HFSS shows 1.015 at 38.1 GHz and 1.01 at 40.1 GHz. Both outcomes indicate excellent impedance matching with minimal signal reflection across the band. The bandwidth for VSWR ≤ 2 aligns with the impedance bandwidth from the S_{11} parameter (≤ -10 dB), further solidifying the agreement between the simulators and validating the design process and simulations.

4.3. Far-field radiation properties

Fig. 18 displays good agreement between CST and HFSS simulation outcomes for the antenna's 2D radiation patterns at 38 GHz and 39.8 GHz in both the E-plane and H-plane. The antenna exhibits a directional radiation pattern with maximum power forward (boresight). The E-plane pattern has a moderately focused beamwidth (45°), while the H-plane has a broader beamwidth (76°). The antenna achieves a gain of 9.03 dBi (CST) and 9.3 dBi (HFSS) at 38 GHz. Similar results with excellent agreement were observed at 39.8 GHz. This consistency highlights the antenna's stable performance across target frequencies.

Fig. 19 reveals radiation efficiency and gain across the operating frequency range (37.23–40.34 GHz). Radiation efficiency stays consistently high (86.97 % to 88.96 %) with a peak of 88.29 % at the center frequency (38 GHz). Gain varies slightly, reaching a maximum of 9.03 dBi at the lowest frequency and dipping to 6.55 dBi at the highest. However, it remains above 9 dBi at the center frequency. This suggests the antenna directs signals most efficiently at lower frequencies within

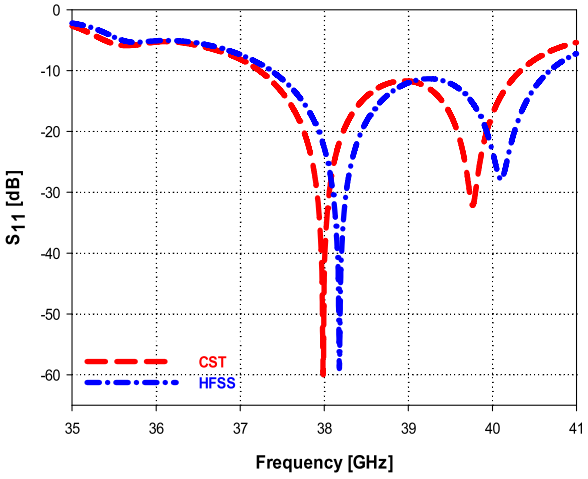

Fig. 16. The simulated S_{11} performance over the operating band using CST and HFSS.

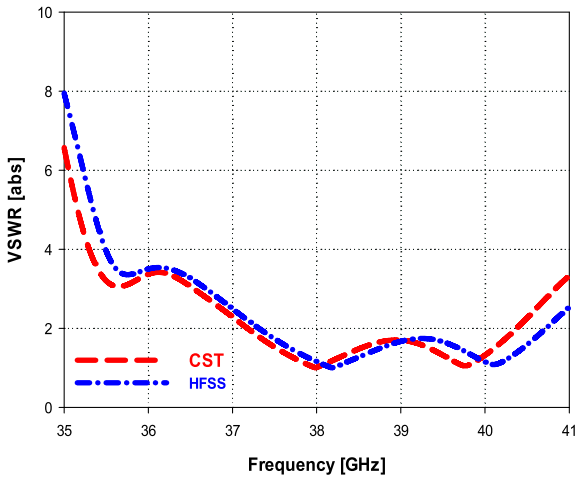

Fig. 17. The simulated VSWR performance against frequency using CST and HFSS.

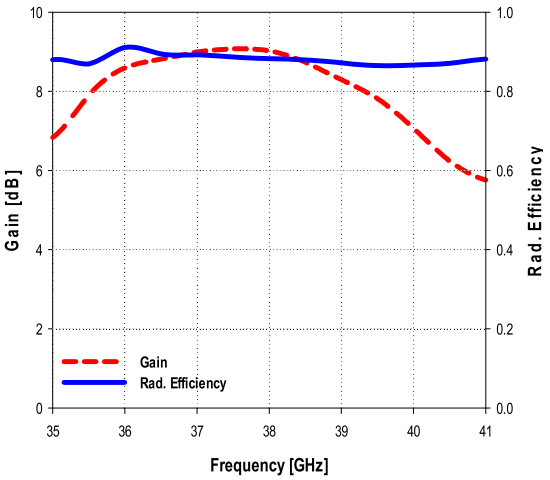

Fig. 19. Gain and radiation efficiency as functions of operating frequencies.

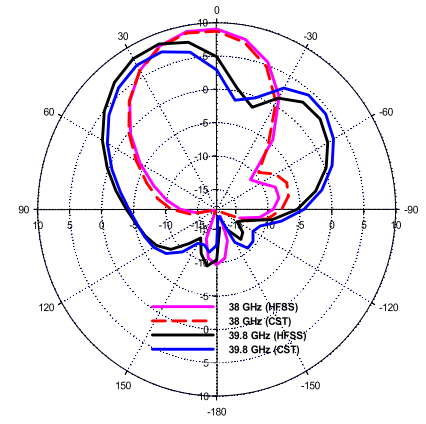

(a) E-Plane

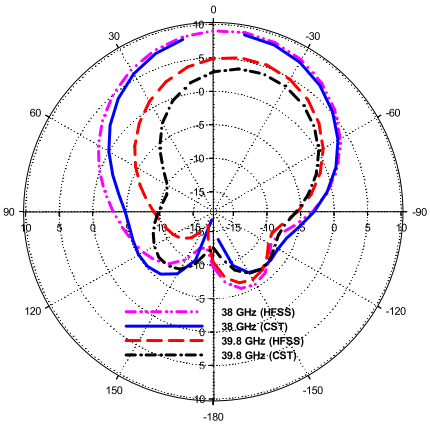

(b) H-Plane

Fig. 18. 2D radiation patterns at 38 GHz and 39.8 GHz using CST and HFSS: (a). E-plane and (b). H-plane.

the band but still maintains sufficient gain for effective transmission across the entire operating range.

4.4. A comparison with some recent published literature

Table I provides a comparison between the antenna design presented in this paper and several designs from recent literature. Our compact antenna design outperforms the established designs in [17–20,32,35,38], and [39] in several key aspects. Notably, it features a much smaller size, making it ideal for space-constrained applications. Additionally, it demonstrates superior signal matching, minimizing power loss, and higher gain, resulting in stronger signal transmission compared to the reference antennas. Although its bandwidth is not the widest overall, it still surpasses the designs in [18–20,35,38], and [39], ensuring efficient operation over a broader frequency range. While the designs in [17] and [32] offer wider bandwidths, our antenna's combination of size, gain, and reflection coefficient makes it the more appealing choice overall. Furthermore, in terms of radiation efficiency, our design stands out, as its efficiency remains nearly constant across the entire operating bandwidth, unlike the other designs listed in Table I, where the reported efficiencies are the maximum values at specific frequencies but decrease across the operating band.

5. Conclusions

A compact design targeting the 38 GHz and 39 GHz bands for 5G applications was presented in this work. To optimize the performance of the proposed antenna, two identical thin rectangular slits were strategically incorporated into the radiating patch. The antenna utilizes a Rogers RT/Duroid 5880 substrate ($\varepsilon r = 2.2$, $\tan\delta = 0.0009$, $hs = 0.186$ mm) due to its favorable electrical properties and is supported by a full ground plane. The optimized design achieved a significant impedance bandwidth of 3.11 GHz (37.23 GHz to 40.34 GHz), ensuring efficient signal transmission across a broad frequency range within the designated band. Excellent impedance matching is evident from the low VSWR of 1.012 and a remarkable S_{11} parameter of −60 dB at the primary resonant frequency (38 GHz), indicating minimal signal reflection and maximized power transfer efficiency. The antenna exhibited promising radiation characteristics, including high gain, making it a strong candidate for 5G applications in the targeted frequency bands. The design and optimization were performed using CST simulation software, and the final design was further validated using HFSS software to enhance confidence in its performance. While the proposed antenna demonstrated promising performance, further research is warranted to refine the design and achieve consistent gain across the entire operational bandwidth.

Declaration of generative Ai and AI-assisted technologies in the writing process

During the preparation of this work, the authors used ChatGPT to check the grammar and improve the readability of the manuscript. After using this tool, the authors reviewed and edited the content as needed

Table 1
Comparison with the recent Literature.

Ref.	[17]	[18]	[19]	[20]	[32]	[35]	[38]	[39]	This Work
f_r (GHz)	28/38	38/60	28/38	38	38	28/38	27/28/33/38	28/38	38
Size (mm^3)	12 × 12 × 0.237	15 × 25 × 0.25	7.5 × 8.8 × 0.25	12 × 12 × 0.203	12 × 11 × 0:9	18 × 8 × 0.25	11 × 11 × 0.25	8.88 × 8.88 × 1.52	5 × 8.2 × 0.186
BW (GHz)	3.8	2	1.06	3	9.2	1.2	1.31	1.28	3.11
Gain (dBi)	4.21	6.5	5.86	5.5	7.81	8.1	8.58	7.8	9.027
S_{11} (dB)	−37.9 @ 38	- 42	- 27.3	- 30	−32	−51.16	−31	−27	- 60
Max. Rad. Eff. (%)	96.6	89.57 @ 38	91.3 @ 38	–	94 (max)	88.8	87.75	93	88.96

and take full responsibility for the final content of the publication.

CRediT authorship contribution statement

AbdulGuddoos S.A. Gaid: Writing – review & editing, Writing – original draft, Validation, Supervision, Methodology, Investigation, Formal analysis, Conceptualization. **Ala'a N.S. Ali:** Writing – review & editing, Writing – original draft, Validation, Software, Methodology, Investigation, Conceptualization. **Mohammad Ahmed Alomari:** Writing – review & editing, Resources, Methodology, Investigation.

Declaration of competing interest

The authors declare that they have no known competing financial interests or personal relationships that could have appeared to influence the work reported in this paper.

Acknowledgments

This research did not receive any specific grant from funding agencies in the public, commercial, or not-for-profit sectors.

Data availability

No data was used for the research described in the article.

References

[1] J.G. Andrews, S. Buzzi, W. Choi, S.V. Hanly, A. Lozano, A.C.K. Soong, J.C. Zhang, What will 5G be? IEEE J. Sel. Areas in Commun. 32 (6) (2014) 1065–1082.
[2] A.G.S.A. Gaid, M.A.M. Ali, A. Saif, W.A.A. Mohammed, Design and analysis of a low profile, high gain rectangular microstrip patch antenna for 28 GHz applications, Cogent. Eng. 11 (1) (2024) 2322827.
[3] B. Bertenyi, 5G evolution: what's next? IEEe Wirel. Commun. 28 (1) (2021) 4–8.
[4] A.S.A. Gaid, A.N.S. Ali, High-gain microstrip patch antenna with a circular slot for WiGig applications in the V-Band, J. Nano Electr. Physics 16 (1) (2024).
[5] S. Agarwal, N.P. Pathak, D. Singh, Concurrent 83GHz/94 GHz parasitically coupled defected microstrip feedline antenna for millimeter-wave applications, in: 2013 IEEE Applied Electromagnetics Conference (AEMC), IEEE, 2013, pp. 1–2.
[6] G. Chittimoju, U.D. Yalavarthi, A comprehensive review on millimeter waves applications and antennas, in: Journal of Physics: Conference Series 1804, IOP Publishing, 2021 012205.
[7] M.A. Khattak, M.I. Khattak, S.M. Owais, A.A. Khattak, A. Sultan, Design and analysis of millimeter wave dielectric resonator antenna for 5G wireless communication systems, Progress In Electr. Res. C 98 (2020) 239–255.
[8] J. Doo, W. Park, W. Choe, J. Jeong, Design of broadband W-Band waveguide package and application to low noise amplifier module, Electr. (Basel)Electr.. (Basel) 8 (5) (2019) 523.
[9] Y. Zhang, A.R. Vilenskiy, M.V. Ivashina, W-band waveguide antenna elements for wideband and wide-scan array antenna applications for beyond 5G, in: 2021 15th European Conference on Antennas and Propagation (EuCAP), IEEE, 2021, pp. 1–5.
[10] A. Saad, M. Ismail, N. Misran, Correlated MIMO Rayleigh channels: eigenmodes and capacity analyses, Int. J. Comput. Sci. Network Security 8 (12) (2008) 75–81.
[11] M. Nahas, A super high gain ʟ-slotted microstrip patch antenna for 5G mobile systems operating at 26 and 28 GHz, Eng. Technol. Appl. Sci. Res. 12 (1) (2022) 8053–8057.
[12] M. Ayari, On the efficiency of the advanced TWA approach to the 60-GHz microstrip antenna analysis for 5G wireless communication systems, Eng. Technol. Appl. Sci. Res. 13 (1) (2023) 10151–10157.
[13] M. Nahas, A high-gain dual-band slotted microstrip patch antenna for 5G cellular mobile phones, Eng. Technol. Appl. Sci. Res. 14 (3) (2024) 14504–14508.
[14] D. Imran, M.M. Farooqi, M.I. Khattak, Z. Ullah, M. Irshad Khan, M.A. Khattak, H. Dar, Millimeter wave microstrip patch antenna for 5G mobile communication, in: 2018 International Conference on Engineering and Emerging Technologies (ICEET), IEEE, 2018, pp. 1–6.
[15] S. Palanivel Rajan, C. Vivek, Analysis and design of microstrip patch antenna for radar communication, J. Electr. Eng. Technol. 14 (2019) 923–929.
[16] El Halaoui Mustapha, L. Canale, A. Asselman, G. Zissis, Dual-Band 28/38 GHz Inverted-F array antenna for fifth generation mobile applications, in: Proceedings 63, MDPI, 2020, p. 53.
[17] A.R. Sabek, A.A. Ibrahim, WA. Ali, Dual-band millimeter wave microstrip patch antenna with StubResonators for 28/38 GHz applications, J. Phys.: Conference Series 2128 (1) (2021) 012006.
[18] M.H. Sharaf, A.I. Zaki, R.K. Hamad, M.M.M. Omar, A novel dual-band (38/60 GHz) patch antenna for 5G mobile handsets, Sensors 20 (9) (2020) 2541.
[19] A.E. Farahat, K.F.A. Hussein, Dual-band (28/38 GHz) wideband MIMO antenna for 5G mobile applications, IEEe Access. 10 (2022) 32213–32223.
[20] A.A. Ibrahim, W.A.E. Ali, M. Alathbah, A.R. Sabek, Four-port 38 GHz MIMO antenna with high gain and isolation for 5G wireless networks, Sensors 23 (7) (2023) 3557.
[21] D.A. Sehrai, M. Asif, N. Shoaib, M. Ibrar, S. Jan, M. Alibakhshikenari, A. Lalbakhsh, E. Limiti, Compact quad-element high-isolation wideband MIMO antenna for mm-wave applications, Electronics. (Basel)Electronics. (Basel) 10 (11) (2021) 1300.
[22] D.A. Sehrai, J. Khan, M. Abdullah, M. Asif, M. Alibakhshikenari, B. Virdee, W. A. Shah, et al., Design of high gain base station antenna array for mm-wave cellular communication systems, Sci Rep 13 (1) (2023) 4907.
[23] J. Khan, S. Ullah, U. Ali, F.A. Tahir, I. Peter, L. Matekovits, Design of a millimeter-wave MIMO antenna array for 5G communication terminals, Sensors 22 (7) (2022) 2768.
[24] A.S.A. Gaid, M.A.M. Ali, Design and simulation of a compact microstrip antenna for 5G applications at the (37–40) GHz Band, Journal of Nano-and Electronic Physics 15 (4) (2023).
[25] M.A.M. Ali, A.G.S.A. Gaid, M.M. Saeed, R.A. Saeed, Design and performance analysis of a 38 GHz microstrip patch antenna with slits loading for 5G millimeter-wave communications, in: 2023 3rd International Conference on Emerging Smart Technologies and Applications (eSmarTA), IEEE, 2023, pp. 1–6.
[26] A.G.S.A. Gaid, M.A.M. Ali, Tri-Band Rectangular Microstrip Patch Antenna with Enhanced Performance for 5G Applications Using a π-Shaped Slot: design and Simulation, Iraqi J. Elect. Elect. Eng. 19 (2) (2023).
[27] A.S.A. Gaid, O.A.S. Qaid, M.A.A. Ameer, F.F.M. Qaid, B.S.A. Ahmed, Small and bandwidth efficient multi-band microstrip patch antennas for future 5G communications, in: Emerging Trends in Intelligent Computing and Informatics: Data Science, Intelligent Information Systems and Smart Computing, 4, Springer International Publishing, 2020, pp. 653–662.
[28] O.Y.A. Saeed, A.A.A. Saeed, A.S.A. Gaid, A.M.H. Aoun, AA. Sallam, Multiband microstrip patch antenna operating at five distinct 5G mm-wave bands, in: 2021 International Conference of Technology, Science and Administration (ICTSA), IEEE, 2021, pp. 1–5.
[29] K.M.A. Kadhar, N. Kumar, S. Tamilselvi, M.Z. Bellary, V. Raja, A. Buradi, B. Vinoth Kumar, A.F. Emma, Single input multiple output maze shaped array antenna for millimeter wave applications, Results. Eng. 22 (2024) 102097.
[30] E. Thakur, A. Gupta, M.K. Abdulhameed, A.D. Khaleel, A.J.A. Al-Gburi, Microstrip antenna with two elements and defected ground structure for 5G mobile applications at 28/38 GHz, Progress in Electromagnetics Res. C 146 (2024).
[31] O. Elalaouy, M.E.L. Ghzaoui, J. Foshi, A high-isolated wideband two-port MIMO antenna for 5G millimeter-wave applications, Results. Eng. 23 (2024) 102466.
[32] I. Shaik, S.K. Veni, Design and analysis of a compact 38 GHz wideband monopole antenna for 5G mm-wave wireless applications, Progress in Electromagnetics Research C 135 (2023).
[33] U. Farooq, A. Lokam, A compact 26/39 GHz millimeter wave MIMO antenna design for 5G IoT applications, J. Infrared, Millimeter, and Terahertz Waves 44 (5) (2023) 333–345.
[34] S. Sadhu, B. Acharjee, S. Mandal, Design of Wideband Microstrip Patch Antenna at 38 GHz for 5G Network, in: International Conference on Data Science and Communication, Springer Nature Singapore, Singapore, 2023, pp. 719–730.
[35] R.R. Elsharkawy, K.F.A. Hussein, AE. Farahat, Dual-band (28/38 GHz) compact MIMO antenna system for millimeter-wave applications, J. Infrared, Millimeter, and Terahertz Waves 44 (11) (2023) 1016–1037.
[36] M. Ahmed, MI. Ahmed, AA. Ibrahim, SM. Gaber, Quad-port 28/38 GHz Antenna with Isolation Improvement for 5G Wireless Networks, J. Infrared, Millimeter, and Terahertz Waves (2024) 1–22.

[37] B. Ghouse, P. Shariff, P. Kumar, PR. Mane, S. Pathan, T. Ali, A-AA. Boulogeorgos, J. Anguera, Dual-Band Antenna at 28 and 38 GHz Using Internal Stubs and Slot Perturbations, Technologies. (Basel) 12 (6) (2024) 84.

[38] RN. Tiwari, K.G Malya, G. Nandini, P.B Nikhitha, D. Sharma, P. Singh, P. Kumar, Quad-Band 1× 4 Linear MIMO antenna for millimeter-wave, wearable and biomedical telemetry applications, Sensors 24 (14) (2024) 4427.

[39] R.H. Elabd, A.J.A. Al-Gburi, Super-compact 28/38 GHz 4-port MIMO antenna using metamaterial-inspired EBG structure with SAR analysis for 5G cellular devices, J. Infrared, Millimeter, and Terahertz Waves 45 (1) (2024) 35–65.